Dynamics of the Oil-Air Interface in Hard Disk Drive Bearings

F. Hendriks[1], *Member, IEEE*, B. S. Tilley[2], J. Billingham[3], P. J. Dellar[4], and R. Hinch[5]

[1]Hitachi GST Corp, Hitachi San Jose Research Lab., San Jose, CA 95120, USA
[2]Olin College of Engineering, Needham, MA 02492 USA
[3]School of Mathematical Sciences, University of Nottingham, Nottingham NG7 2RD, UK
[4]Applied Mathematics at Imperial College London, London SW7 2AZ, UK
[5]Centre for Mathematical Biology, Brasenose College, University of Oxford, Oxford OX1, 4AJ, UK

We study the dynamics of the oil-air interface (OAI) (also called meniscus) of the fluid dynamic bearings of hard disk drives, particularly when the OAI is located among bearing grooves. We derive a simple analytical expression for the evolution of the OAI of an herringbone-type journal bearing. We also report numerical experiments where we include surface tension as a regularization parameter.

***Index Terms*—Fluid dynamic bearing, hard disk drive, spindle.**

NOMENCLATURE

HDD	Hard disk drive.
FDB	Fluid dynamic bearing.
HB	Herringbone.
OAI	Oil-air interface.
BEM	Boundary-element method.
TSD	Tied shaft design.
ODE	Ordinary differential equation.
SG	Spiral groove.

I. INTRODUCTION

IT IS an acknowledged fact that ball bearing spindles of hard disk drives are rapidly being replaced by spindles using fluid dynamic bearings (FDB) [1]. See the nomenclature above for other acronyms used throughout this paper. FDBs have a long history, notably the pioneering work of Muijderman [2] and particularly Bootsma and Tielemans [3]. In FDBs, oil film pressures are created by slanted grooves in either the rotor or stator. We limit ourselves to the study of radial bearings in which the shaft is stationary and does not have any grooves, while the rotor has grooves in the shape of a "herringbone" (HB). The HB grooves move relative to the smooth stator and act as a stalled oil pump. When the spindle does not rotate, the oil is held in the FDB by capillary pressures alone. When the spindle rotates, the location of the oil is dominated by fluid dynamic pressures. In some FDB designs, one or more of the OAIs are located in the HB of the FDB. This is cause for concern because the grooves disturb the OAI. When this disturbing effect is strong enough, small air bubbles may enter the oil, as reported by Asada *et al.* [4]. Once air bubbles are in the FDB, they change the rotordynamics and interfere with normal servo operation of the HDD. Our main goal, therefore, is to investigate the OAI when it is located among the grooves. Fig. 1 shows the lower section of a typical FDB of tied shaft design (TSD) Note that the radial B–C and journal A–B bearings are joined at B. When the rotor R spins around the stationary shaft S, the location of the OAIs is different from those with the spindle at rest. Note that one side of the herringbone section HB is longer than the other to allow the HB pressure to balance the pressure of the spiral groove thrust bearing SG. During spindle operation, the thrust bearing has a capillary buffer C, a tapered reservoir. During standstill, oil also partially fills a capillary buffer adjacent to the HB. In this paper, we only study the upper section of the HB with length.

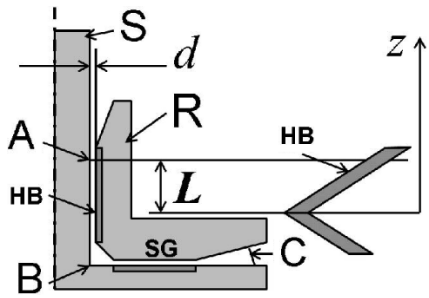

Fig. 1. Cross section of a tied-shaft fluid dynamic bearing. The journal bearing extends from A to B. The thrust bearing extends from B to C. The oil-air interface under study is at A. R: rotor; S: stator; d: bearing radial clearance.

II. PROBLEM DESCRIPTION

We consider the motion of an incompressible viscous fluid between the stator and rotor as shown in Fig. 2. We use a cylindrical polar coordinate system centered at the stator, but a rotating frame of reference in which the *rotor* appears fixed.

In the rotating frame, the stator then appears to rotate backward. The continuity and Navier–Stokes equations are

$$\nabla \cdot \mathbf{u}^* = 0 \tag{1}$$

$$\rho \frac{D\mathbf{u}^*}{Dt} = -\nabla p^* + \mu \nabla^2 \mathbf{u}^* - 2\rho\Omega\hat{\mathbf{k}} \times \mathbf{u}^* - \rho\Omega^2 r\hat{\mathbf{r}}. \tag{2}$$

The asterisks indicate dimensional variables and $\hat{\mathbf{r}}, \hat{\mathbf{k}}$ are the unit vectors in the radial and axial directions, respectively. The last two terms in (2) are the Coriolis and centrifugal forces due to

Digital Object Identifier 10.1109/TMAG.2005.855305

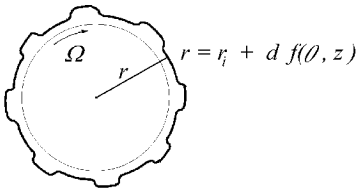

Fig. 2. Rotating coordinate frame. The rotor is rotating with angular velocity Ω in the positive θ direction with respect to an inertial frame. The analysis is expressed in a frame fixed to the rotor in which the grooves are stationary and the stator (shaft) appears to rotate backward.

the rotating reference frame. Referring to Fig. 2, these equations hold in the region $r_i < r < r_i + df(\theta, z), 0 < z < Z(r, \theta, t)$, and $0 < \theta < 2\pi$.

Here, $\mathbf{u}^* = (u_r^*, u_\theta^*, u_z^*)$ is the fluid velocity, with components in the radial, azimuthal, and axial directions respectively, and p^* is the fluid pressure, ρ is the fluid density, μ is the dynamic viscosity, and Ω is the angular rotation speed. The velocity must satisfy no-slip boundary conditions at the inner and outer walls. Thus, $(u_r^*, u_\theta^*, u_z^*) = (0, -\Omega r_i, 0)$ at $r = r_i$ on the stator, while $\mathbf{u}^* = \mathbf{0}$ at $r = r_i + df(\theta, z)$ on the rotor. We impose symmetry conditions on the herringbone centerline. Along the oil-air interface $z = Z^*(r, \theta, t)$

$$\frac{\partial Z^*}{\partial t} - \mathbf{u}^* \cdot \mathbf{n} = 0 \tag{3}$$

$$\sigma \kappa^* = p^* - \hat{\mathbf{n}} \cdot \mathbf{T}^* \cdot \hat{\mathbf{n}} \tag{4}$$

$$[\hat{\mathbf{n}} \cdot \mathbf{T}^*] \times \hat{\mathbf{n}} = 0 \tag{5}$$

where $\mathbf{n} = \nabla[z - Z(r, \theta, t)]$ is the outward normal at the interface ($\hat{\mathbf{n}}$ is the unit vector in the $\mathbf{n}$ direction), σ is the surface tension, κ^* equals twice the mean OAI curvature, and $\mathbf{T}^* = \mu[\nabla \mathbf{u}^* + (\nabla \mathbf{u}^*)^{\mathbf{T}}]$ is the viscous stress. At leading order we have $\hat{p} = \hat{p}(\theta, z, t)$ from the y-momentum equation. Constancy of the pressure across the film and the remaining two momentum equations then lead to a Couette–Poiseuille velocity profile in $y = r - r_i$. Equation (1) at leading order takes the form of Reynolds' equation for an incompressible fluid

$$\frac{\partial}{\partial \theta}\left\{ f^3 \frac{\partial p}{\partial \theta} + 6f \right\} + \frac{\partial}{\partial z}\left\{ f^3 \frac{\partial p}{\partial z} \right\} = 0 \tag{6}$$

where $f(\theta, z)$ denotes the wall profile of the grooved rotor. Homsy [5] shows that a similar argument may be used near the free surface, invoking the notion of a "passive boundary layer." The concept of a single (θ, z) location and velocity of the free interface forces *averaging* of the fluid velocities across y. Assuming that there is a single, coherent OAI, we conclude that the free surface must simply follow the planar velocities imposed by the interior lubrication region where (6) holds. The resulting condition on the interface is

$$\frac{\partial Z}{\partial t} + \bar{u}_\theta \frac{\partial Z}{\partial \theta} - \bar{u}_z = 0 \tag{7}$$

where $Z = Z(\theta, t)$ is the average interfacial height of the OAI, and the average velocity $\bar{\mathrm{u}} = (\bar{u}_\theta, \bar{u}_z)$ is given by

$$\bar{\mathbf{u}} = -\frac{1}{12} f^2 \nabla p - \frac{1}{2} \hat{\theta} \tag{8}$$

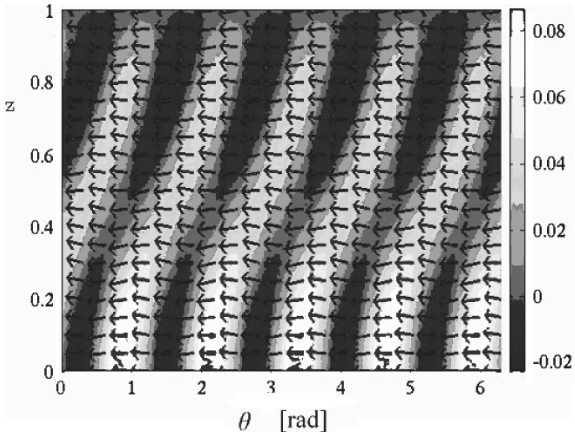

Fig. 3. Pressure distribution and mean flow vectors for the wall profile $f(\theta, z) = 1 + \delta \sin[n(\theta - kz)]$ for $k = 2$ and $n = 5, \delta = 1$.

where $\nabla = (\partial/\partial\theta)\hat{\boldsymbol{\theta}} + (\partial/\partial z)\hat{z}$. The averaging of the normal stress boundary condition results in zero pressure at the interface.

With (8) the kinematic free surface condition, (7) becomes

$$\frac{\partial Z}{\partial t} - \left[\frac{1}{2} + \frac{f^2}{12}\frac{\partial p}{\partial \theta}\right]\frac{\partial Z}{\partial \theta} + \frac{f^2}{12}\frac{\partial p}{\partial z} = 0 \tag{9}$$

subject to the conditions $\partial p/\partial z = 0$ along $z = 0, p = 0$ along $z = Z(\theta, t)$, and p and Z are 2π-periodic in θ.

III. Shallow Groove Limit

Consider the rotor wall profile with shallow grooves

$$f(\theta, z) = 1 + \delta \sin(n[\theta - kz]) \tag{10}$$

where $\delta << 1$ is the amplitude of the rotor wall relative to the mean gap thickness, n is the number of grooves around the rotor circumference, and $k = \cot \alpha$, where α is the groove angle. We expand the pressure and the interfacial deflection terms in a power series in δ. Fig. 3 shows the pressure and the mean flow vectors for this case.

The leading order pressure governed by (9) directly gives us the interfacial deflection

$$\begin{aligned} Z_0(\theta, t) = {} & Z_{\text{in}}\left(\theta + \frac{t}{2}\right) \\ & - \frac{1}{n(1+k^2)\cosh n}\{\sinh n \sin[n(\theta - k)] \\ & + k \cosh n \cos[n(\theta - k)] - k \cos n\theta\} \end{aligned} \tag{11}$$

which yields the magnitude of the OAI deflection as

$$|Z_0|_{Z_{\text{in}}=0} = \frac{k}{n(1+k^2)} \operatorname{sech} n. \tag{12}$$

This clearly shows that *fewer grooves lead to larger deflection*, in agreement with results by Asada *et al.* [4].

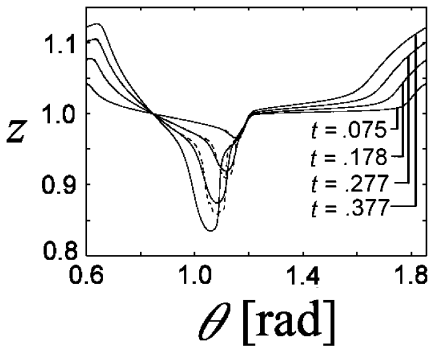

Fig. 4. Evolution of the oil-air interface at various times t for two values of the regularization parameter (surface tension) 10^{-4} (solid line) and 10^{-5} (dashed line). The groove depth is $H = 2$, and the number of grooves is $n = 5$. At $t = 0.075$ the dashed line is indistinguishable from the solid line data. No dashed line data is available for $t = 0.377$. The value of t for each dashed line is that of its nearest neighbor.

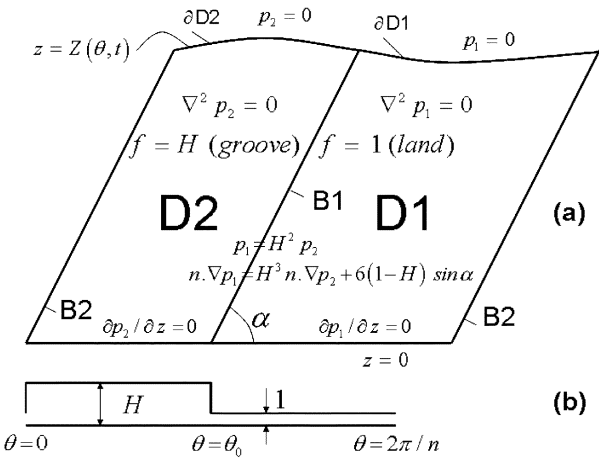

Fig. 5. Equations and domains of solution with piecewise constant grooved surface. (a) shows a view onto the plane of the fluid bearing and (b) shows a cross section of the grooved surface.

IV. Numerical Approaches

A. Fourier/Finite Difference Approach

After mapping the physical domain as follows

$$\eta = \frac{z}{Z(\theta, t)} \tag{13}$$

$Z(\theta, t)$ was obtained by solving a set of ordinary differential equations for its Fourier coefficients using a variable-order ODE integrator [6]. The above model becomes ill-posed in the region of the downward (toward negative z) moving part of the OAI. We reintroduced surface tension as a regularizing parameter to suppress numerical instability. We tested this scheme for a rounded-rectangular groove profile given by

$$f(\theta, z) = 1 + \frac{H}{2}\{1 + \tanh[s[n(\theta - kz)]]\} \tag{14}$$

where s controls the groove profile steepness, $\mathbf{H}$ is the minimum to maximum gap distance (groove depth). Fig. 4 shows the evolution of the free surface for two different values of the regularization parameter $\sigma = 10^{-4}, 5 \times 10^{-5}, \alpha = \pi/3$, and $s = 32$. The groove depth is 2.

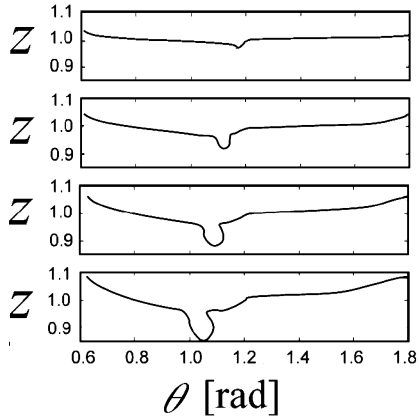

Fig. 6. Free surface "finger" evolution at successive times, computed with the boundary element method. From top to bottom, the time is $t = 0.07, 0.17, 0.27, 0.37$. The settings are $H = 2, z_0 = 1, \theta_0 = \pi/5, n = 5, \alpha = \pi/3$.

B. Boundary Integral Approach

Using the formulation of Fig. 5, interfacial profiles were obtained with the boundary element method (BEM) for piecewise constant f, a common occurrence in FDBs.

The BEM solution method we use is similar to that used by Kelly and Hinch [7]. Fig. 6 shows some computed surface evolutions for a piecewise constant groove profile, again showing a tendency for OAI "fingering."

Acknowledgment

The current paper benefited from helpful suggestions and computational help of T. Marchant, M. Hameed, P. Evans, S. Patel, and D. Tselulko. Hitachi GST supported MPI 2004 held at the University of Delaware, Newark, DE.

References

[1] W. C. Blount, "Fluid dynamic spindle motors: Their future in hard disk drives," IBM Corp., San Jose, CA, White Paper, IBM Storage Systems Group,, 2001.

[2] E. A. Muijderman, "Spiral groove bearings," in *Philips Technical Library*. New York: Springer-Verlag, 1966, ch. 4.

[3] J. Bootsma and L.P.M. Tielemans, "Conditions of leakage-free operation of herringbone grooved journal bearings," *J. Lub. Technol.*, pp. 215–223, 1977.

[4] T. Asada, H. Saitou, Y. Asaida, and K. Itoh, "Characteristic analysis of hydrodynamic bearings for HDDs," *IEEE Trans. Magn.*, vol. 37, pp. 810–814, 2001.

[5] G. M. Homsy, "Viscous fingering in porous media," *Ann. Rev. Fluid Mech.*, vol. 19, pp. 271–311, 1987.

[6] P. N. Brown, G. D. Byrne, and A. C. Hindmarsh, "VODE, a variable coefficient ODE solver," *SIAM J. Sci. Statist. Comput.*, vol. 10, pp. 1038–1051, 1989.

[7] E. D. Kelly and E. J. Hinch, "Numerical simulations of sink flow in the Hele-Shaw cell with small surface tension," *Euro. J. Appl. Math.*, vol. 8, pp. 533–550, 1997.

Manuscript received February 7, 2005.